COBEM2015

ABCM Associação Brasileira de Engenharia e Ciências Mecânicas

23rd ABCM International Congress of Mechanical Engineering
December 6-11, 2015, Rio de Janeiro, RJ, Brazil

ERROR ANALYSIS OF ONE- AND TWO-LEVEL TIME-STEPPING SEMI-LAGRANGIAN INTEGRATORS IN MIXED-FE SPACES

Gustavo Peixoto de Oliveira, gustavo.oliveira@uerj.br
Group of Environmental Studies in Water Reservoirs, State University of Rio de Janeiro, R. Fonseca Teles, 121, São Cristóvão, Rio de Janeiro, RJ, Brazil, 20940-903
Eberson Moraes, ebersonsm@yahoo.com.br
Metallurgy and Materials Engineering Department, Federal University of Rio de Janeiro, Rio de Janeiro, RJ, Brazil, PO Box 68505, 21941-972
José Pontes, jose.pontes@uerj.br
Gustavo Anjos, gustavo.anjos@uerj.br
Norberto Mangiavacchi, norberto@uerj.br
Group of Environmental Studies in Water Reservoirs, State University of Rio de Janeiro, R. Fonseca Teles, 121, São Cristóvão, Rio de Janeiro, RJ, Brazil, 20940-903

Abstract. *Numerical simulations comparing the accuracy of trajectory integrators are presented in this paper through a qualitative error analysis. The core methodology presents one- and two-level schemes to be applied for incompressible flow problems discretised by the Taylor-Hood's MINI element. Emphasis is given to a time-stepping algorithm which seeks intermediary values of the advected quantity to capture precisely the trajectory of particles. Analises are organized regarding numerical tests that bring up the overall differences associated to each of the semi-lagrangian integrators. Comparisons take into account the advection of a scalar concentrate over a two-dimensional domain when submitted to a rotating velocity field, thereby highlighting the advantages of the sub-step integrator for simulating flows that experience, mainly, swirling or curved motions.*

Keywords: *Semi-lagrangian method, finite element, interpolation, numerical algorithm.*

1. INTRODUCTION

Fluid particles traveling amongst stirred fluid motion undergo abrupt changes of position in space. Some examples of such phenomenon occur eventually by diffusion of pollutants over the atmosphere, deposition of contaminant matter on effluents, and mixture of substances in chemical reactions. Consequently, the modelling of the advective transport plays a fundamental role in promoting accurate tracking of particles.

The principal motivation of this work stems from the problem of the chemical dissolution taking place at the inferior border of the working electrode in electrochemical cells, better described as the region of centrifugal expulsion caused by the rotative motion of the cylindrical rod embedded in epoxy resin described in the paper by Barcia *et al.* (2008). Finite element techniques applied to this problem, *e.g.* Anjos *et al.* (2014), have lead the authors of this paper to the study of different semi-lagrangian approaches in FE's scope, such as in Oliveira *et al.* (2015), Oliveira *et al.* (2011a), Oliveira *et al.* (2011b).

Many numerical algorithms to deal with the semi-lagrangian (SL, from now on) advection evolved from finite differences practitioners, e.g. McDonald (1986), Staniforth and Côté (1991), Smolarkiewicz and Pudykiewicz (1992), and Bonaventura (2004) until being integrated into a combined SL/FE methodology by FE's devotees. One of the first insertions of SL/FE codes applied to the Navier-Stokes equations appeared in the work by Pironneau (1982). Later on, other authors published many papers with SL variations for different problems. For instance, studies of convection-diffusion and unsteady problems were carried out by Allievi and Bermejo (2000); a second-order scheme based on a Operator Integration Factor Splitting (OIFS) was implemented by Xiu *et al.* (2005); Discontinuous Galerkin techniques were studied by Restelli *et al.* (2006), to cite a few. More recently, we could cite Henke *et al.* (2014) who developed SL strategies to deal with interface problems discretized by extended finite element (XFEM) spaces and El-Amrani and Seaïd (2012) who used a $\mathcal{L}_2-$ interpolation to circumvent weaknesses found in the classical approaches by calculating trajectories for all the quadrature points belonging to the element.

This paper is focused on the comparison of the accuracy of trajectory integrators based on a SL/FE methodology accomplished by the error analysis between one- and two-level schemes implemented in a mixed scope based on the classical MINI element used to discretize incompressible flow problems Arnold *et al.* (1984). An Adams-Bashfort two-step method is employed to compute intermediary values of the advected quantity to capture precisely the path of particles experiencing, specially, swirling or curved motions. Paper's outline is given as follows: Sec. 2 gives an overview of

the SL method inside the finite element scope as well as of the methodology applied in the numerical results; Sec. 3, in turn, presents qualitative analyses and error comparisons regarding the two trajectory integrators implemented in the computational code. To conclude, Sec. 4 summarizes the main results obtained.

2. SEMI-LAGRANGIAN APPROXIMATION AND FINITE ELEMENTS

2.1 Generalities

Some general concepts are introduced here according to Pironneau (1982) and Ciarlet (1978) in order to relate the SL/FE method in preparation for the coming sections. We denote by $\Omega \subset \mathbb{R}^m$ a spacial domain with boundary $\partial\Omega = \Gamma$ for which $\Omega = \cup_{j=1}^{J} K_j$, with $\mathring{K}_c \cap \mathring{K}_d = \emptyset \ \ \forall c, d$ and simplices K. Furthermore, $\boldsymbol{x}_j, 1 \leq j \leq m+1$ is an element vertex (or a mesh vertex) and the triplet (K, P, Σ) a finite element, for a set of polynomial or quasi-polynomial functions P and a set of degrees of freedom Σ. Additionally, let $\tau = \cup_{n=0}^{N}[t^n, t^{n+1}]$ be the union of finite time intervals, so that $\Delta t = t^{n+1} - t^n$.

2.2 Semi-lagrangian method

The gist of the SL method is to seek an accurate discrete representation of the substantial derivative

$$\frac{D(\cdot)}{D\tau} = \frac{\partial(\cdot)}{\partial\tau} + \boldsymbol{v} \cdot \nabla(\cdot), \tag{1}$$

which is present in several transient systems dominated by advection phenomena, by integrating the characteristic lines $\boldsymbol{X}(\boldsymbol{x}, \tau)$ that solve the differential equation

$$\frac{d\boldsymbol{X}(\boldsymbol{x}, \tau)}{d\tau} = \boldsymbol{v}(\boldsymbol{X}(\boldsymbol{x}, \tau), \tau) \tag{2}$$

backward-in-time through the velocity field $\boldsymbol{v}$ and spatial position $\boldsymbol{x}$. Discretely, a FE-based approximation of Eq. 2 allows us to write

$$\frac{d\boldsymbol{X}_h(\boldsymbol{x}_j, t)}{dt} = \boldsymbol{v}_h(\boldsymbol{X}_h(\boldsymbol{x}_j, t), t) \tag{3}$$

for an $h-$refinement of mesh, so that, when applied to an arbitrary scalar field ϕ, Eq. 1 can be also approximated by

$$\frac{D\phi_h}{Dt} \approx \frac{\phi_h^{n+1} - \phi_{h,d}^n}{\Delta t}, \tag{4}$$

where $\phi_{h,d}^n$ is the value of the field at the so called departure point of the fluid particle's trajectory. The backward-in-time integration stems from the numerical evaluation of the expression

$$\boldsymbol{X}(\boldsymbol{x}, t^n) = \boldsymbol{x} - \int_{t^n}^{t^{n+1}} \boldsymbol{u}(\boldsymbol{X}(\boldsymbol{x}, \tau)\, d\tau, \tag{5}$$

whose simplest first-order approximation in the context presented here is

$$\boldsymbol{x}_d^n = \boldsymbol{x}_j^{n+1} - \boldsymbol{v}_h(\boldsymbol{x}_j^n)\Delta t. \tag{6}$$

More precisely, the SL method is intended to find an optimal approximation through the combination of interpolation/integration techniques for each time step Δt. While the usual attempt is to use a first-order algorithm like Eq. 6 to capture the trajectories of the particles being advected throughout the flow field, higher order methods relating space and time give rise to better choices to model such phenomenon. Generally, the departure point $\boldsymbol{x}_d^n$ does not coincide with a mesh vertex, so that $\phi(\boldsymbol{x}_d^n) = \phi(\boldsymbol{x}_d, t^n)$ should be determined by means of a suitable interpolation provided by the FE spaces.

2.3 MINI element's spaces and interpolation

The MINI element's spaces resort to a combination of function spaces intended to evaluate velocity and pressure fields in a mixed nature of fluid flow simulations whose simplex K_{MINI} is a triangle or tetrahedron. Coupled or decoupled scalar fields, if added to the problem under study, are approximated in the same way as the pressure field. Therefore, in terms of the fluid flow applications envisioned here, the mixed function space associated to the MINI element is given by

$$\mathcal{P}_{MINI} := \mathcal{P}_{\boldsymbol{v}} \cup \mathcal{P}_{\phi}, \tag{7}$$

where $\mathcal{P}_{\boldsymbol{v}}$ is the space of shape functions for velocity and $\mathcal{P}_\phi$ the space of shape functions for pressure and scalar fields - theory on MINI element's spaces is found *e.g.* in (Brezzi *et al.*, 2008, p.69). Similarly, the set of degrees of freedom of this element is given by the union

$$\Sigma_{MINI} := \Sigma_{\boldsymbol{v}} \cup \Sigma_\phi, \tag{8}$$

or

$$\Sigma_{MINI} := \{\boldsymbol{v}(\check{\boldsymbol{x}}), \eta(\boldsymbol{x}_j);\, 1 \leq j \leq m+1\}, \quad m = 2, 3, \;\; \eta = \boldsymbol{v}, \phi. \tag{9}$$

where each $\boldsymbol{x}_j$ is a vertex of the element and $\check{\boldsymbol{x}}$ the centroid, meaning that Σ has up to 14(23) degrees of freedom of velocity and scalar points to be evaluated per element if $m = 2(m = 3)$. In turn, the MINI element is formed by the triplet $(K_{MINI}, \mathcal{P}_{MINI}, \Sigma_{MINI})$.

In the context of the SL approach, interpolations of the physical quantities are required to compute values located at intermediary spacial or temporal positions as seen in Bartello and Thomas (1996) or Bonaventura (2004). Given that $\mathcal{P}_{\boldsymbol{v}}$ is an enriched space with the so-called "bubble functions", a higher order of interpolation is reached for the velocity field whereas the scalar fields are interpolated with linear shape functions. Regarding spacial coordinates - unless exceptions for interpolations over edges that require m nodes -, for an interior point $\boldsymbol{x}^*$ of any mesh element, we compute

$$\boldsymbol{v}(\boldsymbol{x}^*) = \boldsymbol{v}(\check{\boldsymbol{x}})\check{P} + \sum_{j=1}^{m+1} \boldsymbol{v}(\boldsymbol{x}_j)P_j, \;\; \text{with } P, \check{P} \in \mathcal{P}_{\boldsymbol{v}} \quad \text{and} \quad \phi(\boldsymbol{x}^*) = \sum_{j=1}^{m+1} \phi(\boldsymbol{x}_j)Q_j, \;\; \text{with } Q_j \in \mathcal{P}_\phi, \;\; m = 2, 3. \tag{10}$$

2.4 Two-level time-stepping algorithm

It is known that the key steps in the practice of any SL method can be summarized in: i) at a given time t^n, compute for each mesh point $\boldsymbol{x}_j$ an approximate solution of Eq. 2 to determine an estimated departure point and ii) interpolate the quantities required at the intermediary points for posterior advection. Many numerical schemes were combined to calculate both the trajectory integration and interpolation, such as those presented in Allievi and Bermejo (2000), Xiu and Karniadakis (2001) and El-Amrani and Seaïd (2012), in the form of algorithms based on multistep techniques.

An one-level scheme considers a single departure point obtained for each time step $[t^n, t^{n+1}]$ whereas a two-level scheme makes use of a sub-step to correct the linear search and recover a higher order SL alternative on space-time discretization. Two schemes are studied in this paper, namely: SL1, the first-order backward-in-time integrator given by Eq. 6, and SL2, a backward-in-time integrator whose search algorithm is given as follows: for each mesh vertex $\boldsymbol{x}_j$,

- do a backward integration to find the intermediary departure point $\boldsymbol{x}_d^{n-\frac{1}{2}} = (\boldsymbol{x}_d, t^{n-\frac{1}{2}})$;
- interpolate to compute the intermediary velocity $\boldsymbol{v}_h(\boldsymbol{x}_d, t^{n-\frac{1}{2}})$;
- do a second backward integration to find the departure point $\boldsymbol{x}_d^n$;
- compute $\phi(\boldsymbol{x}_d^n)$ by interpolation and advance to the next time step.

This two-step algorithm is written mathematically as: $\forall j = 1, 2, \ldots, J$,

$$I: \quad \boldsymbol{x}_d^{n-\frac{1}{2}} = \boldsymbol{x}_j^{n+1} - \frac{\Delta t}{2}\left[3\boldsymbol{v}(\boldsymbol{x}_j, t^n) - \boldsymbol{v}(\boldsymbol{x}_j, t^{n-1})\right] \tag{11a}$$

$$II: \quad \boldsymbol{v}_h(\boldsymbol{x}_d, t^{n-\frac{1}{2}}) = \boldsymbol{v}(\check{\boldsymbol{x}}^e, t^n)\check{P}^e + \sum_{i=1}^{m+1} \boldsymbol{v}(\boldsymbol{x}_i^e, t^n)P_i^e, \quad \forall \,\text{element}\, e; \tag{11b}$$

$$III: \quad \boldsymbol{x}_d^n = \boldsymbol{x}_j^{n+1} - \frac{\Delta t}{2}\left[2\boldsymbol{v}(\boldsymbol{x}_j, t^n) - \boldsymbol{v}(\boldsymbol{x}_j, t^{n-1}) + \boldsymbol{v}_h(\boldsymbol{x}_d, t^{n-\frac{1}{2}})\right] \tag{11c}$$

$$IV: \quad \phi_h(\boldsymbol{x}_d, t^n) = \sum_{i=1}^{m+1} \phi(\boldsymbol{x}_i^e, t^n)Q_j^e, \quad \forall \,\text{element}\, e. \tag{11d}$$

3. NUMERICAL RESULTS

3.1 Particle trajectory integration

As a primary test, the two-dimensional trajectory of a unique particle was computed by using the SL1 and SL2 algorithms in three tests that consider different time steps (see Table 1) whose results are organized in Fig. 1. The marked points represent the initial positions (stars) from which the particle was traced and the final points (circles) up to the

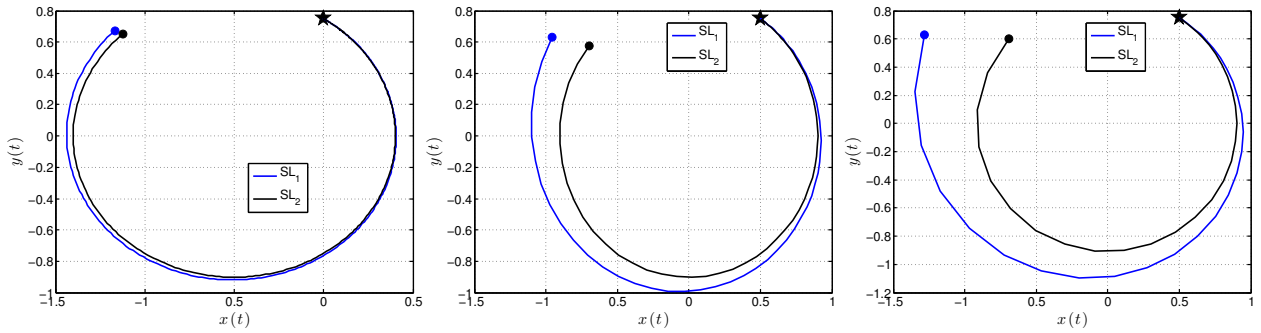

(a) (b) (c)

Figure 1: Comparison of trajectory tracking by the integrators SL1/SL2 for $n \leq \pi/\Delta t$: (a) $\Delta t = 0.01$; (b) $\Delta t = 0.05$; (c) $\Delta t = 0.1$.

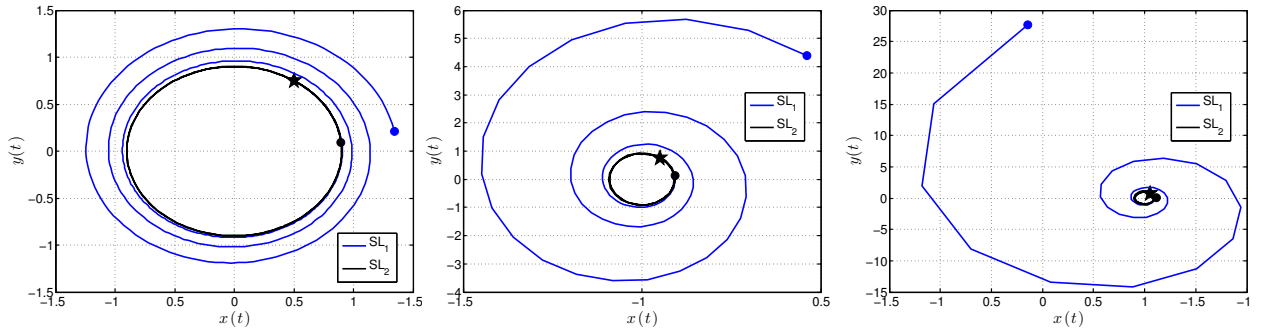

(a) (b) (c)

Figure 2: Comparison of trajectory tracking by the integrators SL1/SL2 for $n \leq 2\pi/\Delta t$: (a) $\Delta t = 0.01$; (b) $\Delta t = 0.05$; (c) $\Delta t = 0.1$.

computation was performed through the SL1 integrator (blue color) and the SL2 integrator (black color) with a number of iterations limited to $n \leq \frac{\pi}{\Delta t}$. Analogously, Fig. 2 depicts the trajectories integrated with a number of iterations limited to $n \leq \frac{2\pi}{\Delta t}$. As seen, the inaccuracy of SL1 to capture the trajectories in comparison to SL2 renders clearer as Δt increases. A relatively high dissipation from the center outward manifests concomitantly the loss of the circular motion imposed by the velocity field, while the integration through SL2 shows a more restrained and less dissipative circular behaviour.

3.2 Concentrate in rotating flow

In a secondary experiment, the advection of a concentrate in rotating flow was implemented in a FE C++ code to afford a more robust numerical analysis. The problem is now described as follows: let $\Omega \times \tau = [0,1]^2 \times [0, T_f]$ be the space-time

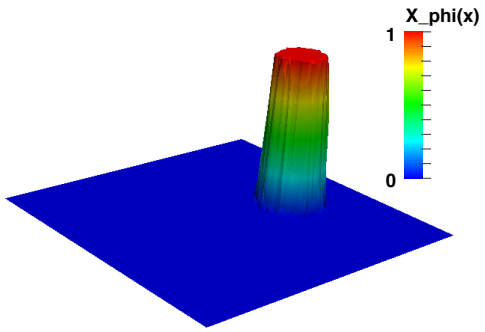

Figure 3: Image of the function $\boldsymbol{\chi}_\phi$ which defines the scalar concentrate region C.

domain of a two-dimensional unit cell and $\boldsymbol{\chi}_\phi(\boldsymbol{x})$ the characteristic function of the scalar concentrate defined as

$$\boldsymbol{\chi}_\phi(\boldsymbol{x}) = \begin{cases} 1, & \text{if } \boldsymbol{x} \in C \\ 0, & \text{otherwise,} \end{cases} \tag{12}$$

Table 1: Testing setup of time step and final angle for the analysed simulations.

Test	Δt	θ_K
1	0.01	3π
2	0.05	3π
3	0.1	$9\pi/2$

where C is a circle of radius $r = 0.1$ with center at $\boldsymbol{x}_C = (0.0, 0.75)$. The region C, represented by the image of $\boldsymbol{\chi}_\phi$ in Fig. 3, is submitted to a rotating flow started up from the rest to a purely advective motion modelled by the inviscid Burgers' equation

$$\frac{\partial \phi}{\partial t} + \boldsymbol{v} \cdot \nabla \phi = \frac{\partial \phi}{\partial t} + y\frac{\partial \phi}{\partial x} - x\frac{\partial \phi}{\partial y} = 0, \tag{13}$$

for $\boldsymbol{v} = (\omega y, -\omega x)$ and a unitary angular velocity ω. Equation 13 is discretized by the MINI FE spaces as discussed previously via the Galerkin method and solved with slip boundary conditions that satisfy $\boldsymbol{v} \cdot \boldsymbol{n} = 0, \;\; \text{at}\, \Gamma = \partial\Omega$, so that $\boldsymbol{\phi}_h(\boldsymbol{x}, t)$ is the approximate field to be analyzed.

3.3 Error analysis

The global relative error E_{θ_k} computed in the $\mathcal{L}_2$-norm was evaluated at certain time instants t^n for which the central point $\boldsymbol{x}_C$ of the rotative concentrate reached the normal angles θ_k and obeys the following expression

$$E_{\theta_k}(\Omega) = \frac{\iint_\Omega \left[\phi_{\theta_k}(\boldsymbol{x}) - \phi_{h,\theta_k}(\boldsymbol{x})\right] \, dxdy}{\iint_\Omega \phi_{\theta_k}(\boldsymbol{x}) \, dxdy}, \quad \boldsymbol{x} \in \Omega, \;\; \text{with} \;\; \theta_k = \theta_C + k\frac{\pi}{2}, k \in \mathbb{Z}_+, \tag{14}$$

for the initial angle θ_C. Only for the test 3, $K = 9$; for the tests 1-2, $K = 3$. Tables 2-4 give an overview of the error E_{θ_k} measured for the SL1 and SL2 methods in the MINI element space. The reason to allow a wider angular displacement for the test 3 stems from the observation of the error behaviour with time in the experiment itself. As expected of SL2, bigger step times produce a more evident improvement over the SL1 integrator. Such assertive is according to the plots in Fig. 4 which, for the test 3, accounts for a mean percentage difference of about 82% in the curves of E_{θ_k}.

Table 2: Error comparison between SL1 and SL2 integrators for the test 1.

Angle (θ_k)	Iteration (n)	E_{θ_k} - SL1	E_{θ_k} - SL2
$\pi/2$	154	0.054310	0.053298
π	313	0.208977	0.205536
$3\pi/2$	470	0.335340	0.331452
2π	630	0.436851	0.429467
$5\pi/2$	785	0.506284	0.498224
3π	943	0.564535	0.556202

Table 3: Error comparison between SL1 and SL2 integrators for the test 2.

Angle (θ_k)	Iteration (n)	E_{θ_k} - SL1	E_{θ_k} - SL2
$\pi/2$	30	0.000011	0.000100
π	62	0.002386	0.001564
$3\pi/2$	93	0.021711	0.013935
2π	125	0.061984	0.041719
$5\pi/2$	156	0.116284	0.076437
3π	188	0.177193	0.119457

Further comparisons can be done by examining the dissipation of the concentrate with time while it travels in a circular-to-spiral motion. Whether the characteristic function is taken as variable, it is observable that the region C

Table 4: Error comparison between SL1 and SL2 integrators for the test 3.

Angle (θ_k)	Iteration (n)	E_{θ_k} - SL1	E_{θ_k} - SL2
$\pi/2$	15	0.000064	0.000014
π	31	0.000128	0.000028
$3\pi/2$	46	0.001375	0.000174
2π	62	0.009521	0.001609
$5\pi/2$	78	0.032484	0.008655
3π	94	0.086187	0.027666
$7\pi/2$	109	0.134180	0.024918
4π	125	0.201191	0.044946
$9\pi/2$	141	0.273773	0.076148

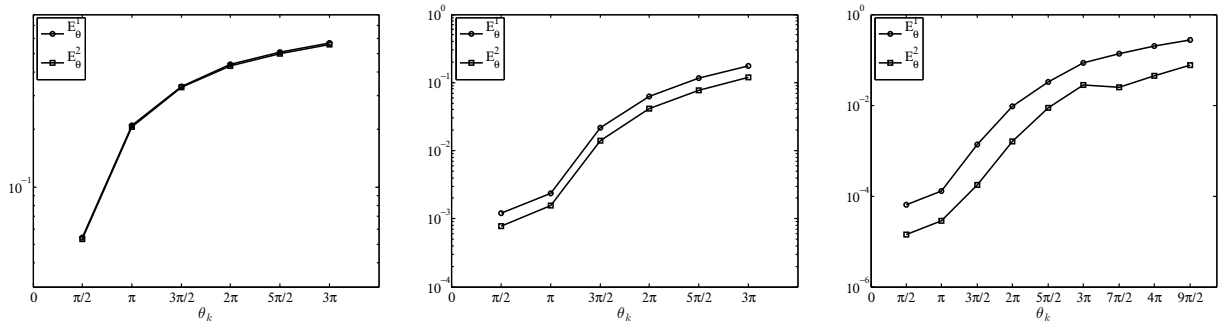

(a) (b) (c)

Figure 4: Error curve E_{θ_k} for each simulation: (a) test 1; (b) test 2; (c) test 3.

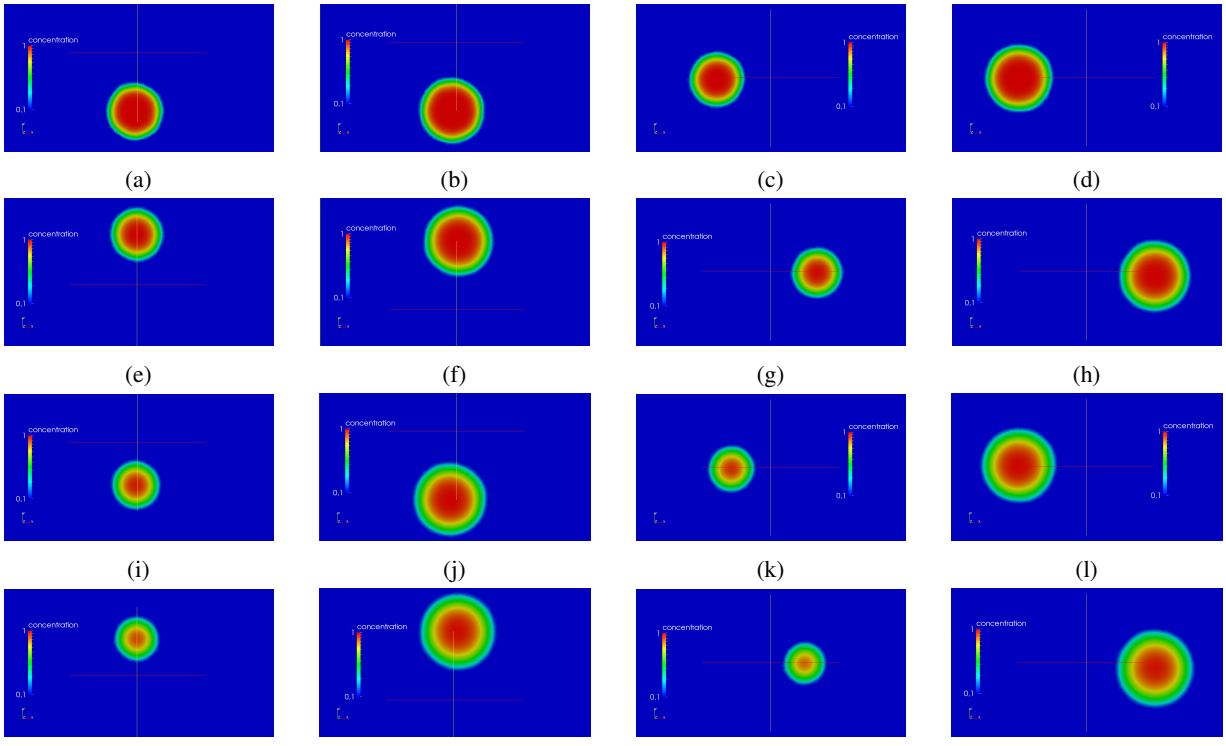

(a) (b) (c) (d)

(e) (f) (g) (h)

(i) (j) (k) (l)

(m) (n) (o) (p)

Figure 5: Comparison of the concentrate dissipation with time for each integrator: (a) $n = 31$ - SL1; (b) $n = 31$ - SL2; (c) $n = 46$ - SL1; (d) $n = 46$ - SL2; (e) $n = 62$ - SL1; (f) $n = 62$ - SL2; (g) $n = 78$ - SL1; (h) $n = 78$ - SL2; (i) $n = 94$ - SL1; (j) $n = 94$ - SL2; (k) $n = 109$ - SL1; (l) $n = 109$ - SL2; (m) $n = 125$ - SL1; (n) $n = 125$ - SL2; (o) $n = 141$ - SL1; (p) $n = 141$ - SL2.

experiences a marked decay of concentration. Figure 5 displays, at left, the image of $\chi_\phi(C)$ on the plane $z = 0$ evaluated for different time instants of the test 3 simulated by calling the integrator SL1, whereas, at right, the image is displayed for the integrator SL2. Besides, note from the Fig. 6 that, for the same test, the initial cylindrical shape of the image of $\chi_\phi(C)$ turns into a "hill" shape along the motion, thus characterizing the higher dissipation of the concentrate for SL1. The pictures refer to frozen profiles of the concentrate over the axis y at $\theta_k = \{\pi, 2\pi, 3\pi\}$.

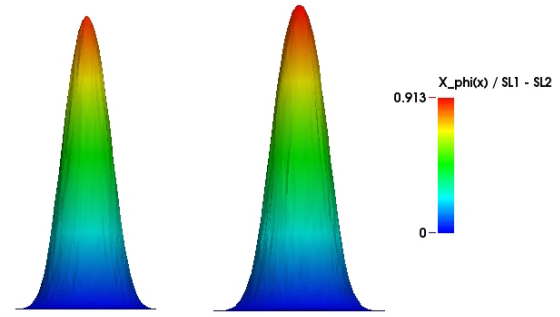

(a)

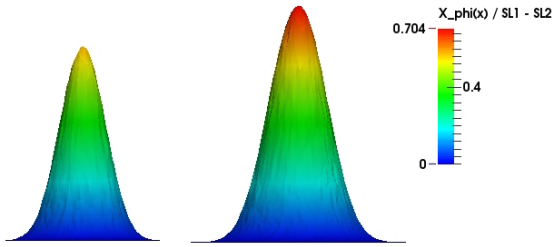

(b)

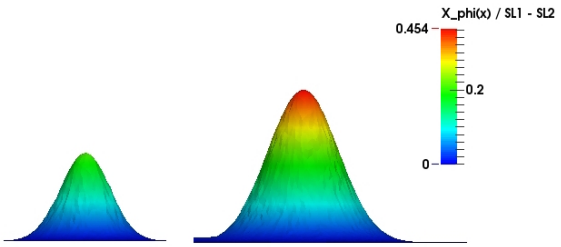

(c)

Figure 6: Frozen profiles of $\chi_\phi(C)$ over the axis y for the SL1 and SL2 integrators (a) $\theta_k = \pi$; (b) $\theta_k = 2\pi$; (c) $\theta_k = 3\pi$.

4. CONCLUSION

This paper studied the advantages of having a two-level scheme intended to model advection phenomena in fluid flow simulations with higher accuracy. By combining techniques of interpolation and integration, the particle trajectories could be traced differently so as to highlight improvements concerning the backward-in-time integration.

A two-dimensional test considered the rotative motion of a scalar concentrate as the framework to analyze the error of the two approaches applied for different time steps. The main conclusion we can draw is that the two-level scheme ensures better accuracy of integration for longer time steps, as expected for a SL method in practical terms. Such result are mainly due to the interpolation method applied which takes intermediary values in space and time.

Although qualitative experiments were reported here, more robust tests as well as numerical analyses are still required in terms of mesh convergence, inclusion of viscous effects, different flow conditions and extension to three-dimensional simulations. Additionally, the study of the SL2 approach for advection of the own velocity field needs to be expanded.

5. ACKNOWLEDGEMENTS

Authors thank to Brazilian agencies CAPES and CNPq for the financial support provided.

6. REFERENCES

Allievi, A. and Bermejo, R., 2000. "Finite element modified method of characteristics for the navier-stokes equations". *International Journal for Numerical Methods in Fluids*, Vol. 32, No. 4, pp. 439–463.

Anjos, G., Mangiavacchi, N. and Pontes, J., 2014. "Three-dimensional finite element method for rotating disk flows". *Journal of the Brazilian Society of Mechanical Sciences and Engineering*, Vol. 36, No. 4, pp. 709–724.

Arnold, D., Brezzi, F. and Fortin, M., 1984. "A stable finite element for the stokes equations". *Calcolo*, Vol. 21, No. 4, pp. 337–344.

Barcia, O., Mangiavacchi, N., Mattos, O., Pontes, J. and Tribollet, B., 2008. "Rotating disk flow in electrochemical cells: A coupled solution for hydrodynamic and mass equations". *Journal of The Electrochemical Society*, Vol. 155, No. 5, pp. D424–D427.

Bartello, P. and Thomas, S.J., 1996. "The cost-effectiveness of semi-lagrangian advection". *Monthly weather review*, Vol. 124, No. 12, pp. 2883–2897.

Bonaventura, L., 2004. "An introduction to semi-lagrangian methods for geophysical scale flows". *Lecture Notes, ERCOFTAC Leonhard Euler Lectures, SAM-ETH Zurich*.

Brezzi, F., Boffi, D., Demkowicz, L., Durán, R., Falk, R. and Fortin, M., 2008. *Mixed finite elements, compatibility conditions, and applications*. Springer.

Ciarlet, P., 1978. *The Finite Element Method for Elliptic Problems*. North-Holland Publishing Company, Amsterdam, Netherlands.

El-Amrani, M. and Seaïd, M., 2012. "A finite element semi-lagrangian method with l2 interpolation". *International Journal for Numerical Methods in Engineering*, Vol. 90, No. 12, pp. 1485–1507.

Henke, F., Winklmaier, M., Gravemeier, V. and Wall, W., 2014. "A semi-lagrangean time-integration approach for extended finite element methods". *International Journal for Numerical Methods in Engineering*, Vol. 98, No. 3, pp. 174–202.

McDonald, A., 1986. "A semi-lagrangian and semi-implicit two time-level integration scheme". *Monthly Weather Review*, Vol. 114, No. 5, pp. 824–830.

Oliveira, G., Mangiavacchi, N. and Pontes, J., 2011a. "Semi-lagrangian high-order 3d interpolation: Survey on a finite element z-type operator". In *Proceedings of the 14th Brazilian Congress of Thermal Sciences and Engineering*.

Oliveira, G., Mangiavacchi, N. and Pontes, J., 2011b. "A semi-lagrangian scheme for fluid flow simulations with a zienkiewicz-type finite element interpolation".

Oliveira, G., Anjos, G., Pontes, J., Mangiavacchi, N. and Thome, J., 2015. "Ale/finite element modeling of an unconfined bubble plume in periodic domain: bubble shape and oscillation analysis". *Journal of the Brazilian Society of Mechanical Sciences and Engineering*, pp. 1–18.

Pironneau, O., 1982. "On the transport-diffusion algorithm and its applications to the navier-stokes equations". *Numerische Mathematik*, Vol. 38, No. 3, pp. 309–332.

Restelli, M., Bonaventura, L. and Sacco, R., 2006. "A semi-lagrangian discontinuous galerkin method for scalar advection by incompressible flows". *Journal of Computational Physics*, Vol. 216, No. 1, pp. 195–215.

Smolarkiewicz, P.K. and Pudykiewicz, J.A., 1992. "A class of semi-lagrangian approximations for fluids". *Journal of the Atmospheric Sciences*, Vol. 49, No. 22, pp. 2082–2096.

Staniforth, A. and Côté, J., 1991. "Semi-lagrangian integration schemes for atmospheric models-a review". *Monthly Weather Review*, Vol. 119, No. 9, pp. 2206–2223.

Xiu, D. and Karniadakis, G., 2001. "A semi-lagrangian high-order method for navier-stokes equations". *Journal of Computational Physics*, Vol. 172, No. 2, pp. 658–684.

Xiu, D., Sherwin, S., Dong, S. and Karniadakis, G.E., 2005. "Strong and auxiliary forms of the semi-lagrangian method for incompressible flows". *Journal of Scientific Computing*, Vol. 25, No. 1-2, pp. 323–346.

7. RESPONSIBILITY NOTICE

The authors are the only responsible for the printed material included in this paper.